The BrIdge voLcanic LIdar—BILLI: A Review of Data Collection and Processing Techniques in the Italian Most Hazardous Volcanic Areas

Stefano Parracino [1] [iD]**, Simone Santoro** [2] [iD]**, Luca Fiorani** [2,*] [iD]**, Marcello Nuvoli** [2]**, Giovanni Maio** [3] **and Alessandro Aiuppa** [4,5] [iD]

[1] Department of Industrial Engineering, University of Rome "Tor Vergata", 00173 Rome, Italy; stefano.parracino@uniroma2.it

[2] Nuclear Fusion and Safety Technologies Department, ENEA (Italian National Agency for New Technologies, Energy and Sustainable Economic Development), 00044 Frascati, Italy; simone.santoro@enea.it (S.S.); marcello.nuvoli@enea.it (M.N.)

[3] BU Space & Big Science, Vitrociset a Leonardo Company, 00156 Rome, Italy; g.maio@vitrociset.it

[4] Dipartimento di Scienze della Terra e del Mare, Università di Palermo, 90123 Palermo, Italy; alessandro.aiuppa@unipa.it

[5] Istituto Nazionale di Geofisica e Vulcanologia, 90146 Palermo, Italy

* Correspondence: luca.fiorani@enea.it

✓ check for updates

Featured Application: Authors are encouraged to provide a concise description of the specific application or a potential application of the work. This section is not mandatory.

Abstract: Volcanologists have demonstrated that carbon dioxide (CO_2) fluxes are precursors of volcanic eruptions. Controlling volcanic gases and, in particular, the CO_2 flux, is technically challenging, but we can retrieve useful information from magmatic/geological process studies for the mitigation of volcanic hazards including air traffic security. Existing techniques used to probe volcanic gas fluxes have severe limitations such as the requirement of near-vent in situ measurements, which is unsafe for operators and deleterious for equipment. In order to overcome these limitations, a novel range-resolved DIAL-Lidar (Differential Absorption Light Detection and Ranging) has been developed as part of the ERC (European Research Council) Project "BRIDGE", for sensitive, remote, and safe real-time CO_2 observations. Here, we report on data collection, processing techniques, and the most significant findings of the experimental campaigns carried out at the most hazardous volcanic areas in Italy: Pozzuoli Solfatara (Phlegraen Fields), Stromboli, and Mt. Etna. The BrIdge voLcanic LIdar—BILLI has successfully obtained accurate measurements of in-plume CO_2 concentration and flux. In addition, wind velocity has also been retrieved. It has been shown that the measurements of CO_2 concentration performed by BILLI are comparable to those carried out by volcanologists with other standard techniques, heralding a new era in the observation of long-term volcanic gases.

Keywords: volcanic eruptions; volcanic plumes; CO_2 flux; DIAL-Lidar; data processing techniques

1. Introduction

Volcanoes represent a significant threat and, at the same time, are a huge attraction since antiquity for populations living nearby due to their fertile lands. At present, large populations live near active or quiescent volcanoes and thus are at risk of their possible eruptions. It is well known that volcanic eruptions can determine increasing air pollution levels; furthermore, they can influence climate [1] and, in some circumstances, produce lethal eruptions that destroy the surrounding environment and cause

serious losses to national/international economies. Cautious valuation of volcano comportment and activity state is required to mitigate these effects, which can be carried out by instruments dedicated to volcanic control [2].

Volcanologists can nowadays infer in real time, by modern technological and modeling developments, the signals coming from seismic and ground deformations that usually happen before eruptions. It is possible to know of an imminent eruption by detecting the stress changes and magma accumulation/flow, thanks to the improvements in broadband seismometers, models, and tools for processing seismic signals [3], and the constant implementation of satellite-based (GPS, Global Positioning System [4] and InSAR, Interferometric Synthetic Aperture Radar [5]) geodetic observations [6].

Volcanic plumes, fumaroles, and degassing grounds release incessantly magmatic volatiles (e.g., H_2O, SO_2, and CO_2) [7], representing the external appearance of deep magma degassing [8,9]. These volatiles are a source of priceless data for forecasting the likelihood of a volcanic eruption. Therefore, accurate knowledge of volcanic gas composition and flux can provide alerts on possible eruptions [10], and provide insights into the geophysical processes occurring in the inner parts of volcanoes.

As far as abundancy is concerned, CO_2 is the second gas in volcanic fluids. Unfortunately, in contrast to SO_2, its measurements are much more complicated. In fact, efforts to achieve standoff detection of the volcanic CO_2 flux have been discouraged by technical challenges. This is mainly due to the large atmospheric background, about 400 parts per million (ppm), which makes it difficult to resolve the volcanic CO_2 signal. For these reasons, there are few volcanic CO_2 flux data in geophysical studies (see [11–14] for fresh research).

In fact, SO_2 can be found at the parts per billion concentration in the unperturbed atmosphere, therefore its volcanic flux can be detected via routinely collected data from the ground (e.g., DOAS, Differential Optical Absorption Spectroscopy [15]) and in space using UV (Ultraviolet) spectroscopy [16–18]. Instead, standoff detection of volcanic CO_2 has only been accomplished during eruptions of mafic volcanoes, where ground-based Fourier transform infra-red (FTIR) spectrometers can take advantage of magma/hot rocks as efficient light sources [19]. Conversely, monitoring of the far more usual "passive" CO_2 releases from quiescent volcanoes has implied access to risky summit craters for direct measurement of fumaroles [20] or in situ sampling of plumes by implementing Multi-GAS (Multi-component Gas Analyzer) systems [21] or Active-FTIR [22].

The employment of modern systems and networks for volcanic gas observations [8,20,23] has made it possible to make significant progress in direct sampling techniques for volcano monitoring. This has resulted in an improvement in time resolution of traditional ground-based volcanic gas observations [24]. Moreover, taking advantage of fast advancements in optoelectronics, especially in the last two decades including new coherent sources, detection systems, and spectrometric devices, we have at present many optical remote techniques, both passive and active, ground-based, airborne, and even space-borne, that are applicable to issues involving Earth CO_2 degassing [12,14]. The improvements of volcanic gas measurements in terms of numbers, quality, and time duration are providing evidence that CO_2 is the gas most directly linked to "pre-eruptive" degassing processes [21]. As confirmation of this fact, precursory increases in CO_2 plume flux have been recently detected at several volcanoes [25] such as at Mt. Etna, the most active and dangerous volcano in Europe [26].

Taking into account the potentialities given by data on the volcanic CO_2 flux for predicting eruptions, the ability to remotely monitor this flux with a high time resolution is an important step ahead in current volcanology.

Considering the stringent requirements of volcanological research and the great advantages of active optical remote sensing (e.g., measurement not dependent of sunlight or other radiation sources, safe monitoring distance, probing of sites difficult to access, large areal coverage, higher accuracy than passive techniques, etc. [14]), ground-based lidar systems have represented, since their creation, a valuable option for the remote detection of volcanic gases and aerosols. Such systems share many advantages with seismic and deformation monitoring with respect to direct sampling; in a nutshell,

they can perform measurements from a safe area, while also allowing (semi)-continuous operation during eruptions. Moreover, gas amounts can be retrieved non-invasively in near real-time, obviating the need for successive laboratory analysis, thus avoiding possible sample contamination, and—unlike in situ sampling—standoff sensing techniques measure integrated or range-resolved gas concentrations through cross-sections of the plume, thus providing a more informative characterization of composition and flux of the volcanic plume [8].

Lidar systems have increasingly been used since the early 1980s for the valuation of volcanic hazards (e.g., during the Soufriere and Mt. St. Helens eruptions in 1979 and 1981, respectively) [8]. Over the last 30 years, several lidars have been deployed to obtain data on the concentrations and fluxes of sulfate aerosol [27–29] and ash [30]. Furthermore, laser remote sensing systems have been used to detect volcanic particles in the troposphere at Mt. Etna (Italy) [31] and in the lower stratosphere during the Pinatubo eruption (Philippines) [32]. In particular, the lidar at Garmisch-Partenkirchen was one of the first examples of volcanic lidar implemented to observe the spread of the stratospheric volcanic plume (from 10 to 28 km) by evaluating the time-series of vertical profiles of the scattering ratio and vertically integrated column of the backscatter coefficient using a Nd:YAG laser operating at 532 nm. These measures were affected by the following average errors: peak scattering ratio: ±4–5% and integrated backscatter coefficient: ±10% [32].

DIAL-Lidar (Differential Absorption Light Detection and Ranging), or simply DIAL, is based on the fast switching of the wavelength of laser pulses on- and off-absorption of the molecule under study. From the application of the Beer–Lambert law to the ratio of the lidar signals (detected radiation vs. range) retrieved at both wavelengths, the range-resolved molecule concentrations (ppm) can be obtained, thus determining the two-dimensional or even three-dimensional plume morphology. This achievement is beyond the capabilities of FTIR, COSPEC (Correlation Spectrometer), and DOAS [15], which provide the path length integrated concentrations (ppm m). DIAL has been deployed at the main Italian volcanoes with UV lasers for tracking the total fluxes of SO_2 [28,33]. In particular, the first example of the quantification of volcanic SO_2 fluxes by using the DIAL (active) technique is reported in [33] where it was extensively compared with passive monitoring techniques (DOAS and COSPEC). In the previously mentioned work, the lidar-based SO_2 fluxes were 50% higher on average than those derived with other standard passive techniques (COSPEC and DOAS) commonly used in volcanology. This mismatch was interpreted as evidence of possible scattering-induced errors in the passive techniques.

More recently, ATLAS (Agile Tuner Lidar for Atmospheric Sensing), a ground-based DIAL system, has been implemented to perform measurements of water vapor flux at the Stromboli volcano (Italy) [34]. To our knowledge, this was the first time that lidar retrieved water vapor concentrations in a volcanic plume.

Finally, the Cloud-Aerosol Lidar with Orthogonal Polarization (CALIOP), an elastic backscatter lidar operated from a satellite, was used to observe volcanic ashes from 15 to 20 April 2010, just after the explosion of the Eyjafjallajökull volcano (Iceland) [35]. This has opened up new scenarios in future volcanic-lidar applications.

However, the apparatuses previously described were costly, heavy, and not effective enough to be implemented in the long-term period. Even though DIAL provides unprecedented opportunities to volcanologists, it requires more advancement to become a reliable technique for routine observations.

In order to fill these gaps, a new DIAL system, designed to measure the volcanic CO_2 flux, was developed as part of the ERC (European Research Council) Starting Grant Project "BRIDGE". The BRIdge voLcanic LIdar (BILLI), assembled at the ENEA (Italian National Agency for New Technologies, Energy and Sustainable Economic Development) Research Center of Frascati by the FSN-TECFIS-DIM group (Diagnostics and Metrology Laboratory) [36], successfully retrieved three-dimensional tomographies of volcanic CO_2 concentration in the plumes at Italy's most hazardous volcanic areas: Pozzuoli Solfatara (Naples, Italy) [21,37,38], the Stromboli volcano (Aeolians Islands, Italy) [39,40], and Mt. Etna (near Catania, Italy) [41,42].

As far as we know, lidar measurements of CO_2 have been performed in volcanic plumes only in recent times, due to the previously mentioned technical challenges and the extreme environmental operating conditions [14,21,37–42]. In the last decade, promising results have been obtained by using a variant of DIAL, known as the Integrated Path DIAL (IPDIAL), but mainly to monitor ambient CO_2 concentrations (e.g., power plants/industrial emissions), and an Open-Path laser Spectrometer (OPS) to measure volcanic CO_2 concentration and flux. However, despite the efforts to provide a remedy to some drawbacks of DIAL-Lidar systems (in terms of costs, complexity of the setup and maintenance, portability and integration time), the aforementioned systems had severe limitations such as the need of a topographic target to perform the measurements of CO_2, which were not range-resolved (only path averaged gas concentrations were retrieved). In addition, the volcanic CO_2 flux computed by OPS was affected by a large uncertainty [14]. Therefore, it can be concluded that BILLI was the first range-resolved DIAL system used to remotely measure both CO_2 concentration and flux in a volcanic plume.

In particular, as will be shown in the following paragraphs, BILLI has been deployed to retrieve range-resolved profiling in wide plumes, thus providing spatio-temporal dispersion concentration maps and high-resolution CO_2 flux time-series. It has opened unprecedented possibilities in measuring volcanic CO_2: BILLI made it possible to clearly detect an excess of a few tens of ppm over a distance of more than 4 km, considering a spatial and temporal resolution of 5 m and 10 s, respectively [42].

Quantifying the CO_2 output from Pozzuoli Solfatara (October 2014) [21,37,38] and Stromboli (June 2015) [39–41] allows for the interpretation, and if possible, the forecast, of the upcoming development of the volcano scenario, with huge benefits to the population living nearby. These examples show the huge social values of lidar systems in monitoring gas emissions. Moreover, observations at densely populated volcanic regions will have a high societal impact throughout Europe. In this regard, the potential of our system has also been confirmed by the results acquired during the last experimental campaign, carried out between July and August 2016 at Mt. Etna [42], retrieving a plume peak beyond 4 km.

The main goal of these experimental campaigns was to measure the exceedance of in-plume CO_2 concentration and flux to provide useful information to volcanological research for a precocious alert to the population in the event of eruptions.

In this paper, after a description of BILLI, special emphasis will be given to data processing and analysis of the experimental results, which will be thoroughly discussed. This was made possible by means of automatic software procedures written in MATLAB and based on the newly designed BRIDGE DIAL data processing technique. Significant CO_2 concentration profiles, dispersion maps, and time-series of CO_2 flux will be shown. Moreover, our monitoring was assessed by conventional data and local meteorological measurements.

Finally, thanks to the BILLI system and from a complete time-resolved plume evolution, it was also possible to retrieve the wind velocity (Stromboli field campaign, 2015), a useful parameter for the CO_2 flux calculation and for the mitigation of volcanic hazards, especially in the field of air traffic security.

2. Materials and Methods

2.1. The BILLI System

A lidar, also known as an optical radar, is an active range-resolving optical remote measurement system whose main components are composed of a transmitter (laser) and the receiver (telescope, optical analyzer/detector, data acquisition/computer). The principle of operation is the following [43,44]: the laser emits a light pulse into the atmosphere and its photons are scattered in all directions from molecules and aerosols (particles, droplets, etc.) present in the air. Part of the light is backscattered toward the telescope. Then, by means of a detector and computer, it is possible to analyze the detected signal vs. The time elapsed between the emission and detection (t). This makes it possible to characterize the chemico-physical properties of air along the beam. In fact, if R is the distance from the

lidar of the backscattering layer and c is the speed of light, we can write R = ct/2. Going back and forth from the backscattering layer, the laser pulse undergoes attenuation by air, as expressed by its extinction coefficient, linked to the light absorption of its species. Often, the absorption lines of molecules are narrow, making it possible to employ DIAL to retrieve their concentration. This technique uses the idea of differential-absorption measurement in which two light pulses with slightly different wavelengths (ON: the light is strongly absorbed by the species under investigation, OFF: the light is not absorbed at all or at least much less) are emitted into the atmosphere, and two corresponding backscattered signals are detected concurrently. The difference between the two profiles is directly linked to the molecule abundance and this technique allows one to determine and map the concentrations of selected molecular species in ambient air [43,44].

BILLI (whose technical scheme and experimental setup are reported in Figure 1) is a monostatic-biaxial DIAL-Lidar system mounted in a small laboratory truck and is composed of a transmitter and receiver equipment [21,37–42].
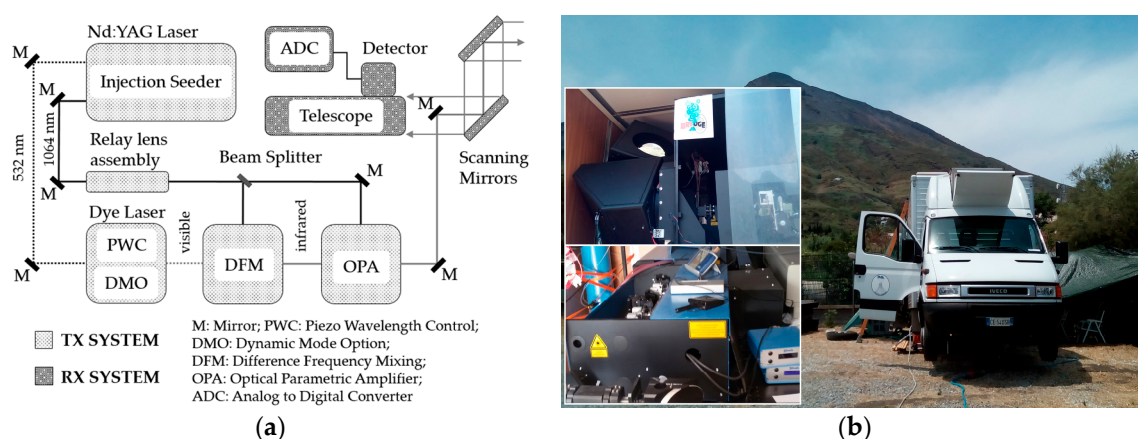
Figure 1. (**a**) Technical scheme of the BILLI DIAL system extrapolated and rearranged from the Figure 2 reported in [37]); (**b**) Experimental setup of the system during the Stromboli campaign (the volcano summit is visible above the two inset pictures). The scanning mirrors and the laser system are visible in the top and bottom inset picture, respectively.

The transmission sub-system is based on a double grating dye-laser optically pumped by an injection seeded Nd:YAG laser (powerful, tunable and narrow-linewidth), a device for the frequency generation (i.e., difference frequency mixing, DFM), and an optical parametric amplifier operating in the NIR (Near IR) band (OPANIR). The limited tunability (few tenths of nm) of Tm, Ho:YLF, and fiber lasers was the main reason of their exclusion (from the transmission sub-system during the implementation stage) given the difficulties in choosing the best absorption line [36]. Instead, due to the harsh environment near degassing craters that can cause burns on the surface of nonlinear crystals, OPOs (optical parametric oscillators) have been discarded [37–39].

This transmitter was used to generate laser radiation at ≈2 μm, a region of the electromagnetic spectrum absorbed by atmospheric CO_2, with negligible cross-sensitivity to H_2O [36].

The laser source of BILLI has the following characteristics [39]:

- 10 pm wavelength stability corresponding to about 0.2 cm^{-1} wavenumber stability;
- enhanced beam profile amplifier (EBPA);
- dynamic mode option (DMO); and
- piezo wavelength control (PWC).

The receiver sub-system is based on a Newton telescope and a detection system, which consists of a thermoelectric-cooled InGaAs PIN photodiode, directly linked to the analog-to-digital converter (ADC). Two large motorized elliptical mirrors (major axis: 450 mm) make it possible to scan all of the

angles above the horizon. The specifications of the whole system are reported in Table 1, and more details are available in previous works [21,37–42].

Table 1. Main specifications of the BILLI system during the BRIDGE field campaigns.

Transmitter	Pulse energy	25 mJ
	Pulse duration	8 ns
	Repetition rate	10 Hz
	Wavelengths	ON: 2009.537 nm, OFF: 2008.484 nm *(Stromboli Volcano 2015, Mt. Etna 2016)*
		ON: 2012.194 nm, OFF: 2011.1 nm *(Pozzuoli Solfatara 2014)*
	Laser linewidth	0.04 cm^{-1}
	Beam divergence	0.5 mrad
Receiver	Mirror coating	Al
	Clear aperture	300 mm
	Focal length	900 mm
	Field of View	1 mrad
Scanning elliptical mirrors	Mirror coating	Al
	Clear aperture	320 mm × 451 mm
Detector module	Photodiode	InGaAs PIN
	Diameter	1 mm
	Responsivity	1.2 A·W^{-1}
	Gain	5.1·104 V·A^{-1}
	NEP	10 pW·Hz$^{-1/2}$
	Bandwidth	0–10 MHz
Analog-to-digital converter (ADC)	Dynamic range	14 bit
	Sampling rate	100 MS·s^{-1}

From Table 1, it is possible to note that, with respect to the Pozzuoli Solfatara field campaign [21,37,38], the operative wavelengths were slightly changed during the campaign carried out at Stromboli and Mt. Etna [39–42]. This was due to the different mode of operation of the system.

In fact, in the first campaign, the line (2012.194 nm) was selected looking for low cross-sensitivity to water vapor and high absorption coefficient [37,38] that was optimum for short-range measurements of CO_2 concentration, whereas, in the other cases, the main goal was to reach longer ranges. To do this, the differential absorption cross section of carbon dioxide ($\Delta\sigma$) was reduced and a different ON line (2009.537 nm) was chosen [39,42]. For more details, see Table 2 [21,37–42].

As will be shown in the following, it was observed that the measurement uncertainty was governed by instability in the wavelength set. For this reason, from the Stromboli campaign, a photo-acoustic cell—with CO_2 at atmospheric pressure and temperature—was mounted at the laser output, thus providing wavelength accuracy, repeatability, and stability, as has been shown in the laboratory [36–42].

Table 2. Wavelengths, wavenumbers, and CO_2 absorption coefficients calculated (at T = 296 K, P = 1 atm) during the field campaigns of Pozzuoli Solfatara, Stromboli volcano, and Mt. Etna.

	Pozzuoli Solfatara, October 2014		Stromboli Volcano, June 2015 and Mt. Etna, July 2016	
Mode	ON	OFF	ON	OFF
Wavelength [nm]	2012.194	2011.1	2009.537	2008.484
Wavenumber [cm^{-1}]	4969.7	4972.403	4976.271	4978.880
CO_2 Abs. Coeff. [m^{-1}]	7.474	0.331	1.934	0.302
CO_2 Δσ [m^{-1}]	7.143		1.632	

Moreover, a new version of the software was developed: the step motor that modifies the resonator cavity inside the dye laser now allows one to shift the emitted wavelength, and the photo-acoustic signal was measured, averaging for 1 s (i.e., for 10 laser shots). In this way, the wavelength shown by the laser monitor can be corrected for a small shift (0.12 cm^{-1}) and the experiment and theory [45] agreed within the linewidth of the emitted pulse (0.04 cm^{-1}). This leads to being able to control the wavelength with the photo-acoustic cell before every lidar measurement, so that the operator can fix the ON and OFF wavelengths with a smaller error than the emitted linewidth [39].

Therefore, a gradual refinement of the system performances was obtained in the last two in-field campaigns, thanks to the following measures:

- an appropriate choice of CO_2 absorption cross section, which enabled both short- and long-range measurements;
- the implementation of the photo-acoustic cell, resulting in a containment of systematic uncertainty associated with measurements of CO_2 concentration (see Section 2.2.5); and
- the reduction of the laser beam divergence due to a better optical setting, resulting in an improvement in the signal-to-noise ratio (SNR).

As will be shown in the following, this allowed us to detect CO_2 plume peaks beyond 4 km and to improve the accuracy of the CO_2 flux measurements. Finally, efforts have been spent to improve the system portability and, in particular, to integrate existing data processing routines [42].

Summarizing, the main characteristics of the system are as follows:

- the lidar is able to explore the troposphere in both vertical and horizontal directions;
- every lidar return is obtained averaging at least 50 shots ON and OFF (interlaced between them with t$_{shift}$ = 0.1 s);
- the temporal resolution of the lidar echoes (Δt) is about 10 ns, corresponding to a ΔR of 1.5 m, although the actual time resolution of BILLI is 5 m: this latter value corresponds to the time response of the detection system and is linked to its bandwidth [39]);
- a concentration profile can be obtained in about 10 s by a couple of lidar signals (ON and OFF) using the newly designed mathematical technique explicitly developed for this application;
- starting from lidar signals of the same scan, it is possible to retrieve the dispersion map of in-plume CO_2 concentration (ppm) in the investigated area;
- knowing the (estimated) plume velocity, it is possible to obtain the carbon dioxide flux (Kg·s^{-1}) [21,41,42]; and
- starting from lidar profiles acquired successively, it is possible to track the motion of discrete atmospheric particles emitted by the volcanic crater, and this allows one to also estimate the wind velocity [38] (more details are reported in Section 3.2).

However, a comprehensive overview of the special features of BILLI has been reported in previous works [21,37–42].

2.2. The BRIDGE DIAL Data Analysis Technique

As above-mentioned, from the literature [44], it is well known that the radiation returned to the lidar telescope vs. time is linked to the backscattering of the laser pulse by an atmospheric layer at a specific range from the system. Consequently, lidars provide range-resolved characterization of the atmosphere and of its components (particulates and molecules) along the path of the laser pulse. This information can be displayed by means of intensity vs. distance graphs.

Considering that for our experiments a DIAL system was deployed, two different wavelengths—λ_{ON} and λ_{OFF}, absorbed and not absorbed, respectively, by carbon dioxide—were used to acquire the intensity profiles. The difference between the two wavelengths was very small and, as a consequence, the behavior of the atmosphere (e.g., considering aerosol and molecular attenuation and turbulence effect on the beam transmission) was the same, except from the CO_2 absorption. Thanks to the difference in return between the nearly simultaneous λ_{ON} and λ_{OFF} signals (as stated in Table 1, the time interval between two successive laser pulses was 0.1 s), and using the previous mentioned technique, the operator can retrieve the range-resolved CO_2 concentration profile in volcanic plumes.

The BRIDGE DIAL technique is a mathematical procedure written with MATLAB software that has been specifically developed for real-time data processing and graphic presentation of data, acquired during the field campaigns carried out by the BILLI system. As recalled before, throughout the years, both the system and the data analysis technique have been optimized. In this section., only the main steps of the technique are reported, and more details are given in previous works [21,37–42].

2.2.1. Preliminary Steps

Generally, raw data are: (i) normalized by dividing the lidar signal by the laser energy; and (ii) background-noise subtracted [44]. Background noise here is measured by averaging the farthest part of the lidar echo (see Figure 2a(1)).

To simplify, during its travel to distance R, the pulse energy decreases: (i) exponentially, due to air extinction; and as $1/R^2$, simply because the detected photons are directly proportional to A/R^2 (i.e., the solid angle of the telescope), where A is its effective area. To compensate for this effect, the lidar signal P(R) (where P is the received power as a function of range R) is commonly transformed into the range-corrected signal (RCS). This is performed by multiplying the signal P(R) by R^2 [44] (see Figure 2a(2)).

Finally, to further improve the SNR (Signal-to-noise Ratio), up to 100 laser shots have been averaged for every lidar return and a Savitzky–Golay filter [46] algorithm with 13 points was used (see Figure 2a(2)).

2.2.2. Conversion of RCS (Range Corrected Signal) Profiles Into Range-Resolved Profiles of in-Plume Excess CO_2 Concentrations

The core of the BRIDGE DIAL technique consists of the following steps [21,37–42]:

- Evaluation of CO_2 concentration in the natural background atmosphere (C_0) outside the plume [39].
- Evaluation of the average excess CO_2 concentration (ΔC) in the volcanic plume cross-section (e.g., between two rockfaces as shown in Figure 1 [39]) encountered along the laser optical path in the examined region with respect to C_0.
- Calculation of the range-resolved excess of in-plume CO_2 concentration, corresponding to each i-th ADC channel of the lidar profile from (see Figure 2b):

$$C_{CO_2,i} = \; k \cdot RCS_i \tag{1}$$

$$k = \frac{\Delta C(R_1 - R_2)}{\Delta R \sum_i RCS_i} \tag{2}$$

where k is the multiplication factor; ΔC—as we mentioned—is the average excess carbon dioxide concentration measured between the two rockfaces and is inferred from the ratio of the corresponding two lidar echoes; R_1 and R_2 indicate the ranges of the two rockfaces; ΔR is the range interval corresponding to an ADC channel; and RCS is the range corrected signal.
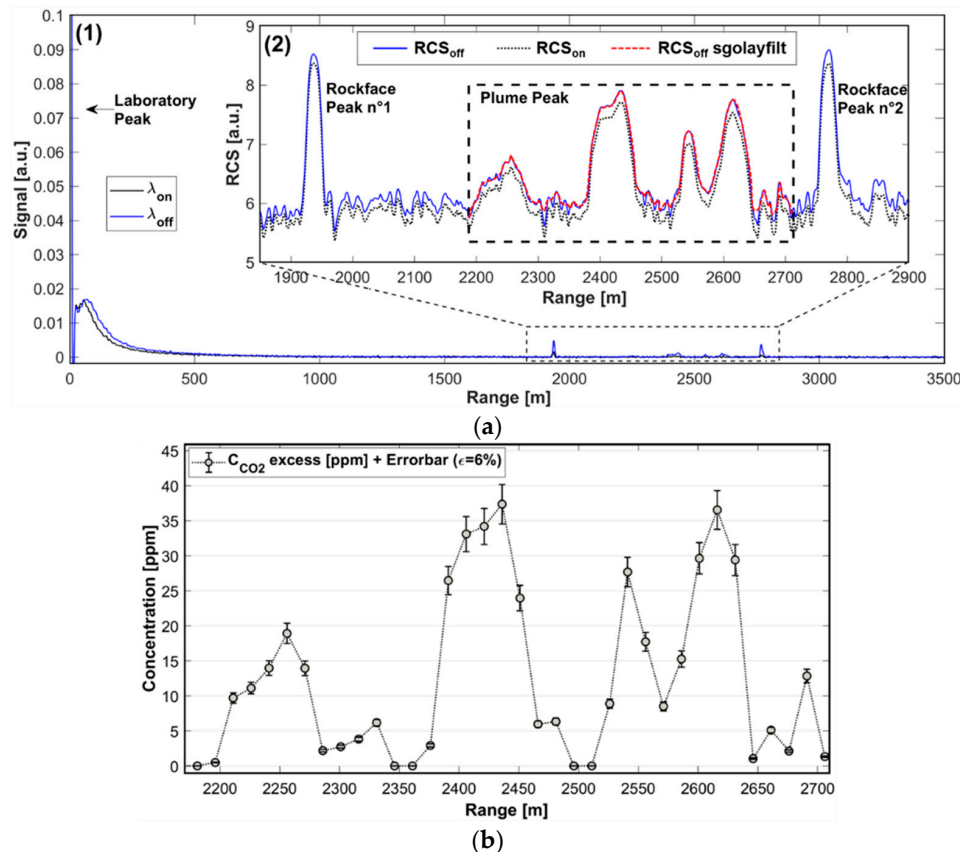
Figure 2. (**a**) Example of a lidar profile acquired during the Stromboli volcano field campaign on 26 June 2015. (1) Data profiles in the form of signal intensity (arbitrary units, a.u.) vs. range (in meters) cleaned by the noise. (2) Detail of the experimental RCS (Range Corrected Signal) and filtering of the OFF channel using a Savitzky–Golay filter algorithm with 13 points in which the plume peak is visible between two rockfaces in the range interval between 1800 and 2900 m. The laboratory peak in (1) provides the start time of the pulse emission and is due to the reflection of some laser radiation inside the mobile laboratory. The two rockface peaks (2), as their name indicates, are due to pulse backscattering by the rockfaces of Stromboli. Finally, the peaks from 2200 to 2700 m are linked to the backscattering of the laser pulse from the plume. (**b**) Particulars of the exceedance of in-plume CO_2 concentration profile (acquired at 11:27, with an elevation 16.98° and azimuth 237.8°). The quadratic sum of statistical (2%) and systematic (5.5%) uncertainties led us to estimate an overall uncertainty of about 6%.

It should be noted that, during the in-field preliminary setup, the system was optimized to perform measurements in selected directions, where one or more topographic targets were partially inside the lidar FOV (Field of View). This allowed us to retrieve some useful parameters (see C_0, ΔC, and k) for the initialization of the data analysis technique. Once the multiplication factor is known, it is possible to perform sequential measurements multiplying each range-corrected lidar profile by this factor, within the limits of the expected dispersal area of volcanic plume.

- Drawing CO_2 dispersion maps by scanning the selected region and arranging subsequent concentration profiles (acquired at different scanning angles and relative to the same scan) in chronological order.

2.2.3. Assessment of the Plume Transport Velocity

The plume velocity v_p (m·s^{-1}) can be inferred from UV camera photograms [21,41,42] or assessed by implementing the correlation method [40,47].

The latter case consists of the following main steps [40]:

- Firstly, RCS is normalized by the laser emitted energy on a shot-per-shot basis (see Table 1) to define a normalized signal $S(R_i)$ independent of the energy fluctuation. Then, the mean normalized signal $\bar{S}(R_i)$ is obtained by averaging N successively recorded individual signals at successive times t_n.

- Second, once we know $S(R_i)$ and $\bar{S}(R_i)$, it is possible to retrieve the information about the shot-per-shot fluctuations of the signals, with respect to the mean normalized signal that is contained in the fractional deviations (specific datasets in which the time evolution of in-plume spatial aerosols inhomogeneities is clear) as:

$$f(R_i, t_n) = \frac{S(R_i, t_n) - \bar{S}(R_i)}{\bar{S}(R_i)} \tag{3}$$

- Third, to determine the displacement of the backscattering inhomogeneities, a cross-correlation function $\rho(L, \Delta H)$ is defined with respect to an altitude interval ΔH and to a lag value L, corresponding to a discrete number of spatial points as:

$$\rho(L, \Delta H) = \frac{1}{\sigma \sigma_L} \sum_{i=a}^{b} \sum_{n=1}^{N-1} f(R_i, t_n) f(R_{i+L}, t_{n+1}) \tag{4}$$

and a superimposed Gaussian estimator is employed on the data to calculate the mean and standard deviation values. These values, respectively, are used to infer the radial wind velocity and its uncertainty.

- Finally, it is possible to measure the horizontal component of the wind velocity (in this kind of application, the vertical component of wind can be neglected) as:

$$v = \frac{v_r \cos \theta}{\cos \Delta \Phi} \tag{5}$$

where v_r is the radial wind in the altitude interval ΔH determined from the lag value for which the correlation is maximum; θ is the elevation angle of the telescope; and $\Delta \Phi$ is the difference in the azimuthal orientation of the wind vector and of the light path.

It should be noted that the described experimental technique (for the tracking of wind velocity) has the advantage of being performed remotely, rapidly, and without additional costs, thanks only to a further data processing routine integrated in the main data analysis software. Therefore, using the same dataset, BILLI is able to perform multiple measures of in-plume CO_2 concentration (in excess), flux, and simultaneously, a good estimation of the plume transport velocity over large areas. This can also be useful to provide a fast tracking of volcanic ash, in order to improve air traffic security. Nevertheless, although promising results (in line with in-situ weather stations) have been obtained using the correlation method, the main drawbacks are still high measurement uncertainty and discrepancy with respect to other optical devices (e.g., UV camera images), probably due to the high fluctuations of wind as a function of the altitude and the differences between the devices and/or data acquisition/processing techniques [40].

2.2.4. Evaluation of CO_2 Flux

The values of CO_2 concentrations reported both in the profiles (see Figure 2b) and the dispersion maps (see Figure 3a, Figure 4a, Figure 5b) were used to compute the carbon dioxide flux (see Figure 3b, Figure 4b, Figure 5c). To this aim, it is necessary to integrate the excess (i.e., background corrected) carbon dioxide concentrations over the whole cross-section of the plume determined by each scan, and multiply this amount by the transport velocity of the plume. Formally, the carbon dioxide flux (Φ_{CO_2}, in $Kg \cdot s^{-1}$) is calculated from the following equation [21,41,42]:

$$\Phi_{CO_2} = v_p \cdot \frac{PM_{CO_2}}{10^3 N_A} \cdot N_{molCO_2-total} \tag{6}$$

where v_p is the plume transport velocity ($m \cdot s^{-1}$); $N_{molCO_2-total}$ is the total plume carbon dioxide concentration ($molecules \cdot m^{-1}$); and PM_{CO_2} and N_A are the CO_2 molecular weight and the Avogadro's constant, respectively. $N_{molCO_2-total}$ was calculated by integrating the effective average excess CO_2 concentrations ($\overline{C_{exc,i}}$ in ppm) over the whole plume cross section, according to:

$$N_{molCO_2-total} = N_h \cdot 10^{-6} \cdot \sum_i \overline{C_{exc,i}} \cdot A_i \tag{7}$$

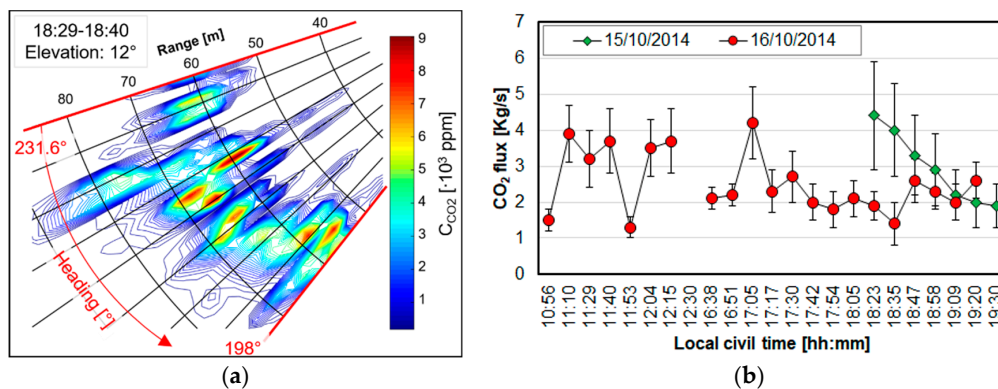where N_h is the atmospheric number density [$molecules \cdot m^{-3}$] at the crater; 10^{-6} converts it into parts per million (ppm); and A_i represents the i-th effective plume area provided by:

$$A_i = l_i \cdot \Delta R \tag{8}$$

where ΔR is the ADC resolution (1.5 m) and l_i is the i-th arc of the circumference:

$$l_i = R_i \cdot \theta \tag{9}$$

where R_i is the i-th range vector (m) and θ is the angle resolution (rad).

(a)　　　　　　　　　　　　　　　　　　　　　　(b)

Figure 3. (**a**) An example of a lidar scan in polar coordinates through the plume at an elevation of 12° (15 October 15 2014). The contour lines show isopleths of background-corrected CO_2 mixing ratios in the plume (expressed in ppm, the legend is the vertical colored bar), shown as a function of heading and range. (**b**) Time-series of lidar-derived CO_2 fluxes from Pisciarelli obtained from 15 October (afternoon) to 16 October (afternoon), rearranged from Figure 4 reported in [21]. The timescale for the morning scans on 15 October is shown in green. Each point refers to a particular scan through the plume (time is the onset time of the scan, with each scan lasting 10–20 min) [21].
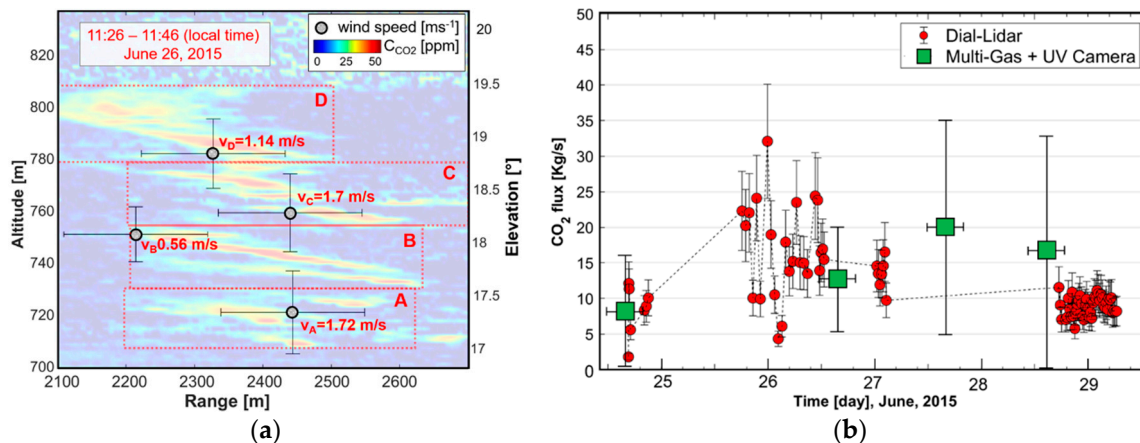
Figure 4. (**a**) In-plume CO_2 concentration map acquired on 26 June 2015 at Stromboli. Carbon dioxide concentration varies as a function of increasing altitude (on the left of the map) and elevation (on the right of the map). The superimposed grey points represent the vertical wind profile retrieved by BILLI in the same dataset. Here, the mean value of the wind velocity was found about 1.3 m/s. The x-axis error bar is the weighted average standard uncertainty of wind velocity, equal to 0.52 m/s. Instead, the error bar on the y-axis represents the altitude halfwidth between adjacent regions (A, B, C, and D) [40]. This figure has been obtained by combining Figure 4 and Figure 8 reported in [40]. (**b**) Time-series of CO_2 fluxes from Stromboli volcano from 24 to 29 June 2015, rearranged from Figure 5 reported in [41]. The BILLI based fluxes (red circles) were obtained using the procedure detailed here [39,41]. For comparison, independent CO_2 flux estimates, obtained by multiplying the in-plume CO_2/SO_2 ratio (from Multi-GAS) by the SO_2 flux (from UV cameras) are also presented (green squares) [41].

2.2.5. Evaluation of Uncertainty Sources

The main sources of uncertainty that affected our CO_2 flux measurements are reported below [39,41]:

1. Systematic uncertainty of the carbon dioxide concentration measurement. Taking into account the experience [21,41], the systematic uncertainty of the BILLI system was dominated by inaccuracies in wavelength setting [39], and this led to errors in differential absorption cross section and, as a consequence, in CO_2 mixing ratio. In this regard, in order to control the transmitted wavelength before each atmospheric measurement, a photo-acoustic cell filled with pure CO_2 (at atmospheric pressure and temperature) was implemented close to the laser exit. This allowed setting the ON/OFF wavelengths used in this study with an accuracy better than the laser linewidth [39], with an overall uncertainty in the wavelength setting equal to $\pm$ 0.02 cm^{-1} (half laser linewidth). For these reasons, the systematic uncertainty of the CO_2 concentration measurement was below 5.5% [41,42].

2. Statistical uncertainty of the carbon dioxide concentration measurement. Starting from the calculation of the standard deviation of the signals corresponding to every ADC channel, and implementing the standard uncertainty propagation technique [48], it has been possible to evaluate the statistical uncertainty. This uncertainty varies as a function of distances from the system, considering typical atmospheric and plume conditions encountered during field campaigns. Typical values at 2.5 km and over 4 km from the system were estimated to be equal to 2% and slightly above 5%, respectively [41,42].

3. Uncertainty linked to plume transport velocity. Mean and standard deviation of the wind velocity were calculated, also in this case by the standard uncertainty propagation technique. Then, the corresponding relative uncertainty was evaluated [48]. The assessed values ranged from 3% (at Stromboli [41]) to 19% (at Pozzuoli [21]).

4. Uncertainty in the characterization of the integration area. Due to difficulties in accurately assessing the surface where there is an excess of carbon dioxide concentration, this parameter

represented the main source of uncertainty for the calculation of volcanic CO_2 fluxes, with an order of magnitude estimated to be about 25% [41].

If all uncertainty sources are statistically independent, all the components have to be quadratically summed [48] in order to obtain the total uncertainty of volcanic CO_2 fluxes, which varies from 20% to 30% (dominated by the area uncertainty [41,42]). This value is consistent with the results obtained during the field campaigns of Pozzuoli (2014) [21], Stromboli (2015) [41], and Mt. Etna (2016) [42].
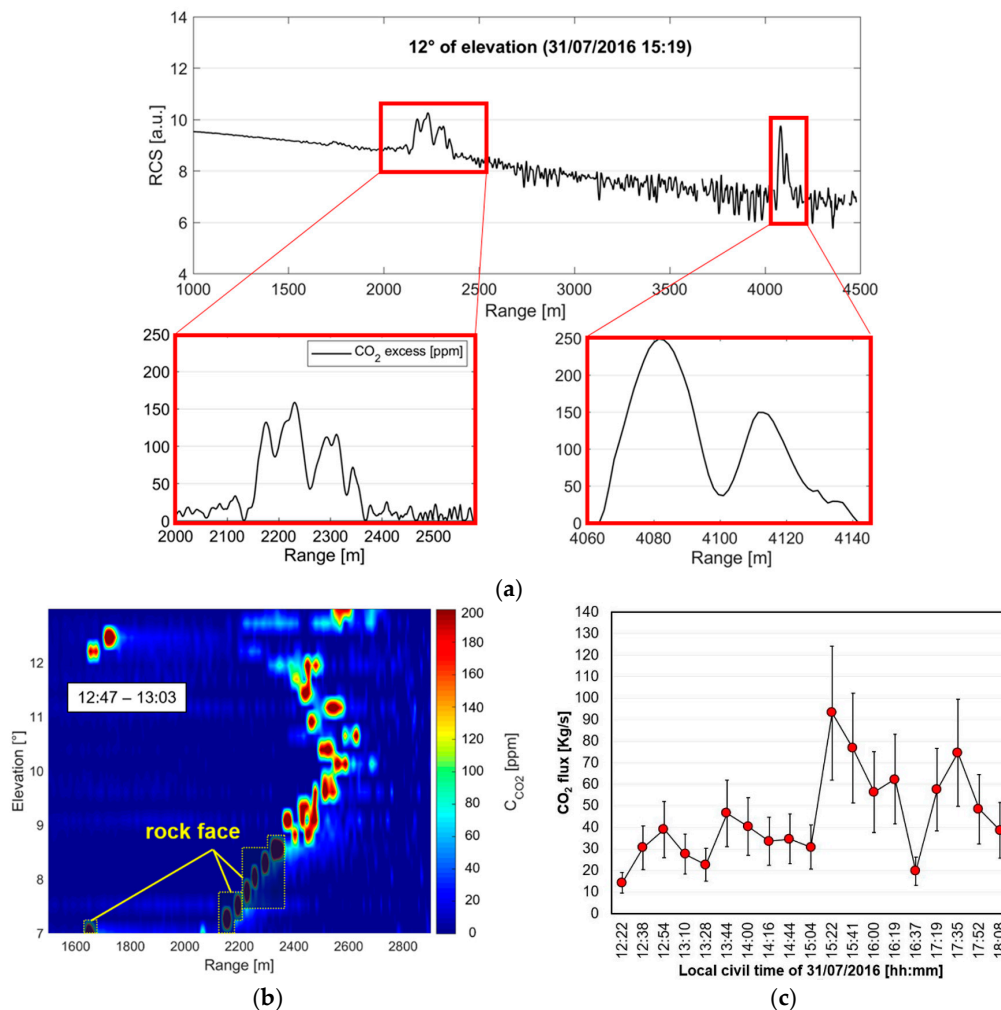
Figure 5. (**a**) Lidar return at 12° of elevation: two wide and jagged peaks from the volcanic plume are clearly visible; the CO_2 profiles inside the volcanic plume are shown in the two red boxes. The uncertainty was equal, respectively, to 6% for the left-side plume peak and 7.5% for the right-side plume peak. (**b**) Vertical scan (fixed azimuth: 230°) of the volcanic plume (CO_2 excess) acquired on 31 July 2016 (12:47 p.m.–1:03 p.m., local civil time). With that fixed azimuth and in the elevation range 7–9°, rockfaces reflect the laser pulse, corresponding to peaks that are not linked to the plume (rockfaces are disentangled from plume because of the narrowness of peaks). (**c**) Carbon dioxide flux measured at the northeast crater on 31 July 2016 (12:22 p.m.–6:08 p.m., local civil time). The bars show the error in carbon dioxide flux (33%). Please note that the previous figures were extrapolated and rearranged from Figure 2a, Figure 4c, Figure 5, respectively, reported in [42].

3. Results and Discussion

A brief overview of the experimental campaigns carried out over three years by the BILLI system will be presented and discussed here.

The first experimental campaign was carried out during October 2014. The system was placed ≈100 m far from the fumaroles of Pozzuoli Solfatara (Pisciarelli, Phlegraen Fields). The system performed a horizontal scan at different elevations, retrieving, for the first time, CO_2 concentration dispersion maps and time-series of lidar-derived CO_2 fluxes [21,37,38].

About ten months later (June, 2015), other tests were carried out at Stromboli Volcano Island, where BILLI operated nearly 24 h for almost a week, performing horizontal and vertical scans. CO_2 excess of a few tens of ppm was measured in some minutes in the volcanic plume up to a distance of nearly 3 km far from the system. In addition, in this case, daily cycles of CO_2 flux were successfully retrieved [39–41].

Finally, the potential of the BILLI DIAL system was confirmed by the last field campaign at Mt. Etna at the end of July 2016, where, for the first time, in-plume CO_2 concentration peaks were retrieved at a distance exceeding 4 km [42].

It should be noted that during all field campaigns, eye safety regulations were followed and weather did not alter the BILLI operation, except for a moderate influence of the wind, as is reported in Section 3.2 [21,37–42].

3.1. The Experimental Campaign of Pozzuoli Solfatara

The first field experiment was conducted at the Phlegraen Fields volcano [21,37,38]; this is a rising caldera including Pozzuoli and the suburbs of Naples, among the most inhabited zones of Italy. The bradyseismic crises of the volcano produced thousands of shallow earthquakes, and its activity has been often, even if not continuously, active in the last few decades. Scientists and stakeholders observed these recent crises, despite them not evolving into an eruption, bearing in mind the related important hazard mitigation problems and the linked necessary interventions. These issues have become even more critical taking into account that ground uplift restarted in 2012, with the intensification of degassing activity, in the caldera center and at the main surface hydrothermal manifestations of Solfatara and Pisciarelli. Current uplift/degassing unrests observed in Pozzuoli are probably due to intermittent injections of carbon dioxide-rich gas in the hydrothermal system of the volcano, indicating that fresh magma is supporting a strong inflow of gas from deep layers. Here, attention has been focused on the degassing fumarolic vent of Pisciarelli that, besides a small augmentation in discharge temperature (from less than 95 °C up to 110 °C), has visibly escalated in degassing activity over the past decade (the carbon dioxide concentration in fumaroles has also risen), making it the most active among the Italian fumarolic vent areas. Therefore, quantifying the CO_2 output from Pisciarelli is vital for the interpretation and possibly the prediction of future changes in this volcanic zone [21].

The system measured nearly continuously during both 15 and 16 October 2014, after the experimental setup on 14 October. During the measurement operations, BILLI performed a horizontal scan of the almost vertical plume in the 198°–232° range of azimuth angles (see Figure 3a). The elevation of 12° was used mostly for the performed scans, where the plume structure was fully resolved and the lidar echoes were more intense. Controls proved that at lower and higher elevations, the plume was often either optically too thick or too spread, so only a few additional scans at 0°, 6°, and 15° were completed. A total of 200 lidar returns (100 at λ_{ON} and 100 at λ_{OFF}, see Table 2) were ascribed to a single profile and averaged to improve the SNR; in this way, the sampling frequency of the lidar echoes was 0.05 Hz, which corresponded to a 20-s time resolution. As already discussed, the space resolution of BILLI was 5 m. The combination of about 25 profiles yielded a total scan of the plume in around 10 min [21,37,38].

Thanks to the BRIDGE DIAL technique (see Section 2.2) it was possible to retrieve, globally, up to 40 scans of CO_2 concentration in excess in the plume and, at the same time, the CO_2 flux time-series. The whole dataset covered almost three days of operation, for a maximum of nine consecutive hours. Examples of the CO_2 dispersion map and flux time-series are reported in Figure 3a,b, respectively [21].

Figure 3a illustrates the results of a typical scan (using the polar diagram) through the plume. When the laser beam intercepted the plume, peak CO_2 concentrations of up to 5000 ppm were measured.

The plume was typically crossed at azimuth angles of 205–225° and at distances in the range of 50–70 m from the system. At azimuth angles <205° and >225°, or at distances <50 and >70 m, BILLI retrieved the carbon dioxide concentration usually found in ambient air, thus providing confirmation that the laser beam was able to scan the whole plume. This result directly corresponded to the most vigorously degassing fumarolic vent of Pisciarelli. An evident CO_2 peak, in scans performed at an elevation angle of 6°, was even clearer in the same fumarolic vent. This fact was also due to the reflection of the laser beam off the rockfaces enclosing the vent [21,37,38].

Figure 3b, instead, illustrates CO_2 flux time-series from the fumarolic system. Here, the cross-correlation analysis, applied to sequences of visible images of the moving plume that were co-acquired at a high rate (30 Hz) by a digital optical camera, was applied to achieve the vertical plume transport velocity. The overall error in the calculated plume velocity was in the range from 10 to 28%, leading to a total error of CO_2 fluxes from 15 to 33% [21].

Thanks to the high time resolution (around 10 min) of the system, it was possible to follow important intraday dynamics, nearly impossible to measure with conventional instruments for several reasons such as environmental difficulties, high costs, instrumentation ineffectiveness, and the larger amount of ambient air carbon dioxide that is present along the line of sight between the spectrometer, target (plume), and the source of photons (sun, magma, and lava fragments).

The strong changes over timescales of tens of minutes are clear in the Pisciarelli hydrothermal site such as from a peak emission of 4.4 Kg/s (at 18:23 h local civil time on 15 October) down to 1.9 Kg/s after about 60 min. Apart from these fast variations, our data indicate a general constancy of CO_2 output over timescales of a few days. The mean carbon dioxide emissions for 15 and 16 October 2014 were quite similar (2.63 ± 0.98 and 2.52 ± 0.84 Kg/s), corresponding to the total daily outputs of 256 ± 89 and 218 ± 71 tons, in that order. Furthermore, the carbon dioxide fluxes measured by BILLI were in overall agreement with other estimations carried out with in situ data obtained with a portable gas analyzer [21].

Nevertheless, our system has the following advantages: (i) external light sources are not required; (ii) measurements can be performed without risk from a remote area; (iii) the spatio-temporal resolution is finer; and (iv) the morphology of the plume can be obtained in some minutes.

Moreover, the big difference between the lidar echoes coming from the plume and ambient air allows the operator to disentangle the carbon dioxide of volcanic origin, and therefore to quantify the volcanic carbon dioxide flux. Such measurements are new in geophysics, and promise to contribute to volcanological research.

Even though, at this experimental stage, a considerable number of further developments are needed (e.g., system miniaturization, automation, independent measurements of in-plume wind velocity, and long-distance remote sensing), the system performed the first measure of CO_2 concentration and flux in a volcanic plume [21].

3.2. The Experimental Campaign of Stromboli Volcano

The second field experiment was conducted at Stromboli Volcano Island. The volcanic activity on the island is generally considered "regular" and mild (strombolian). Larger-scale vulcanian-style explosions occasionally occur. Although these events, locally referred to as "major explosions" or "paroxysms", are not frequent and are short-lived (from tens of seconds to a few minutes), they could be extremely dangerous for locals and authorized personnel, since they produce fallout of coarse pyroclastic materials over wide dispersal areas. Moreover, neither geophysical nor volcanological precursor signals were observed before these events occurred. This could be due to the fact that they originate deep in the crustal roots of the volcano plumbing system. However, it has been observed that the previously cited events are systematically preceded by days/weeks of anomalous CO_2-rich gas leakage from the Stromboli's deep (8–10 km) magma storage zone. For these reasons, volcanologists are considering with increasing interest CO_2 flux emissions from the open-vent crater plume for the monitoring of volcanic activity and hence for the assessment and mitigation of the related hazards [41].

As in other volcanic areas, at Stromboli, the volcanic gas CO_2 from a combination of simultaneously measured SO_2 fluxes and plume CO_2/SO_2 ratios has also been recently evaluated [7,11]. Even though the remote measure of SO_2 flux is possible by implementing UV spectroscopy [16], the CO_2/SO_2 ratio requires in situ direct sampling/measurements close to hazardous active vents. For the previous reasons, the implementation of the BILLI DIAL system for the remote observation of the volcanic CO_2 flux, from distant and less risky locations, is a real advantage.

The system operated almost continuously from 24 to 29 June 2015 despite the harsh environmental conditions due to the presence of high humidity, acid vapors, and re-suspended dust. It was placed inside the fence of the local ENEL (main Italian electric company) power plant in the Scari area, ≈2.5 km from the degassing vents on the volcano summit, between the margins of morphological peaks known as Pizzo and Vancori, 918 and 924 m, respectively, above sea level (ASL). The laser beam typically scanned the azimuth angles from 235.3° to 253.6° and the elevation angles from 15.2° to 27.4°.

As stated in Section 2.1, in order to reduce the differential absorption cross section of CO_2, the transmitted wavelengths were changed with respect to the previous campaign (see Table 2). As a result, longer distances were reached by the laser beam. Furthermore, the implementation of a photo-acoustic cell filled with pure CO_2 allowed us to reduce the systematic uncertainty, dominated by instability in wavelength setting, to 5.5% (see Section 2.2.5). Compared to the previous experimental campaign, the pulse repetition rate remained unchanged (10 Hz), instead both the temporal resolution was slightly modified and set at 10 s because only 100 lidar returns (50 at λ_{ON} and 50 at λ_{OFF}, interlaced) were averaged for each scan to increase the SNR. A further improvement of the SNR and, therefore, of the accuracy of both CO_2 concentration and flux measurements was possible by employing filtering algorithms and curve fitting techniques, in the preliminary data analysis steps (see Section 2.2.1). Furthermore, by combining about 50 profiles, it was possible to obtain both vertical and horizontal plume scans in less than 10 min. Eventually, by processing several repeated scans (usually 10) acquired at different elevations, we also retrieved three-dimensional tomographies of the volcanic plume [39–41].

Thanks to an improved and fully automated version of the BRIDGE DIAL data processing routine (taking into account local conditions and the changes in system setup), it was possible to retrieve up to 180 scans of CO_2 concentration in excess in the plume and, at the same time, the CO_2 flux time-series. In addition, thanks to a further data processing routine (see Section 2.2.3), it was possible to estimate the plume transport velocity and, hence, the local wind velocity. The whole dataset covered almost six days of operation, for a maximum of 12 consecutive hours. Examples of CO_2 dispersion map, wind profiles, and flux time-series are reported in Figure 4a,b, respectively [39–41].

Figure 4a illustrates the results of a typical vertical scan through the plume as a function of range (X axis), elevation angle, and altitude (Y axes). The tomography reported above was extrapolated from the measurement session performed on 26 June 2015 between 11:26 and 11:46 (local civil time), and it represents a dataset acquired as a single group of measurements slowly stepping up in elevation angle (from 16.8° to 20°) over the course of about 20 min, since, during that time, the plume displacement was extremely clear. The carbon dioxide concentration in the zone under study is indicated by the color scale, with peaks exceeding 60 ppm. Here, the volcanic plume was encountered in the 2150−2600 m range, from 17 to 19.5° elevation angles, and a fixed azimuth of 237.8°. Regions highlighted with red boxes and named as A, B, C, and D were posited to be the same set of scatterers being tracked over time. Therefore, they represent a useful example for summarizing the time evolution of inhomogeneities relative to the volcanic plume. To appreciate these displacements, it is necessary to specify that particles detected in region A need a certain amount of time to move to the regions B (about 3 min), C (about 6 min), and D (about 9 min). As observed in the field, these movements were mainly due to the presence of wind blowing from north–northwest [40].

Considering both vertical and horizontal scans of the whole campaign, the beam hit the plume at azimuth angles in the range 237–251°, elevation angles in the range 16.5–20° (which means altitude of 700–830 m) and at distances in the range 2200–2500 m. For azimuth angles <237° and >251°, or for distances <2200 and >2500 m, BILLI retrieved the carbon dioxide concentration we usually find

in ambient air, thus providing confirmation that the laser beam was able to scan the whole plume. This result was confirmed by direct observations [37,39].

The quality of the results (as in the example shown in Figure 4a), combined with the high temporal resolution of the acquired data, allowed us to perform, almost simultaneously with in-plume CO_2 concentrations, the first independent measurement of plume transport velocity (v_p) and therefore of the wind velocity, using the correlation method mentioned in Section 2.2.3 and detailed in a previous work [40]. As already mentioned, the assessment of the wind velocity could be crucial for both the CO_2 flux retrieval and air traffic control applications. In this regard, a set of data (lasting about 90 min) was selected from the morning of 26 June 2015.

An example of vertical wind profile was superimposed on the same dataset (lasting about 20 min) of the CO_2 concentration dispersion map reported in Figure 4a, showing a high consistency with the time evolution of the in-plume spatial aerosol inhomogeneities (see the previously mentioned A, B, C, D regions highlighted with red boxes).

The global weighted average value of wind velocity was found equal to 1.1 ± 0.4 m/s for the whole measurement test session. Although promising in terms of cost saving and speed, our measurements were slightly different from the ones acquired by the UV camera [41] and affected by a high uncertainty level due to the presence of wind blowing in the perpendicular direction, with respect to the system location, the worst observing condition for the tracking of the wind [40]. Nonetheless, they were found in agreement, within the error bar, with weather data acquired by conventional devices and with a precision comparable to that of stand-alone fixed-beam correlation lidars. It should be noted that, a comprehensive comparison with local data was considered unreliable, since the nearest weather station on the island performed 6-h average of weather parameters acquired at 4 m ASL and not at the same height of the laser beam pointing. For these reasons, efforts will have to be devoted to advance the configuration of BILLI (e.g., implementing at least three beams or a 360-degree scanning mirror) to fully and accurately retrieve the three components (x, y, and z) of the wind velocity [40]. Therefore, due to the constraints (in terms of dataset duration and results reliability) of our preliminary tests on the fast tracking of wind velocity, during the Stromboli campaign, CO_2 flux time-series were retrieved using v_p values obtained from processing the sequences of UV camera images [41].

Once having obtained the CO_2 dispersion maps and the plume transport velocity using the method described in Section 2.2.4, it was possible to retrieve the CO_2 flux time-series with a cumulative uncertainty equal to 25% (dominated by the integration area uncertainty), as reported in Figure 4b [41]. The results confined the CO_2 flux during 24–29 June 2015 in the range from 1.8 ± 0.5 to 32.1 ± 8.0 Kg/s. The daily mean values of CO_2 flux were obtained by averaging all successful results for each measurement day. The values range from 8.3 ± 2.1 (24 June) to 18.1 ± 4.5 (25 June) Kg/s and corresponded to daily emissions of 718 and 1565 tons, in that order. These data are in agreement with past carbon dioxide estimates carried out at Stromboli. Moreover, in Figure 4b, our lidar-based CO_2 fluxes were compared with alternative measurements, obtained by multiplying the CO_2/SO_2 ratio by the SO_2 flux, which is obtained using the traditional Multi-GAS + UV spectroscopy-based techniques. Despite the issues of the Multi-GAS + SO_2 flux approach reported in the literature (distinct temporal resolutions, and poor temporal alignment [41]), we found a general agreement between the CO_2 fluxes obtained by BILLI and the usual instruments. This provided reciprocal trust for both techniques. Furthermore, BILLI-based carbon dioxide fluxes showed a better temporal resolution (≈16–33 min) and greater continuity. Moreover, BILLI as well as other standoff instruments, is intrinsically safe for operators [41].

In conclusion, although several improvements were made (higher distances reached, fully automated operational routines, independent measurements of plume transport velocity) with respect to the previous campaigns [39–41], efforts were needed to improve the system (in particular, improving portability and reducing power requirements). At the same time, further in-field tests were still necessary to fully explore the potential of our system, validating the reliability and efficiency of the data analysis method.

3.3. The Experimental Campaign of Mt. Etna

The last experimental campaign was carried out at Mt. Etna Volcano (3329 m ASL), a hostile and only partially inhabited region located near Catania, in Sicily. Mt. Etna is the largest and most important volcano in Italy and one of the most active volcanoes in the world. For these reasons, it was the ideal place to test our system performances [42]. Similar to previous campaigns, the main goal was to measure the exceedance of in-plume CO_2 concentration and flux to provide useful information to volcanological research for a precocious alert to the population in the case of eruptions.

The area chosen for our experiments was the northeast summit crater of the volcano (other craters were discarded due to fact that volcanic plume is too dilute or only partially visible) and is characterized by extremes of temperature, high humidity, and rates of rainfall, and the presence of acid vapors, re-suspended dust and particles, which are toxic for humans and dangerous to the instrumentation. Notwithstanding the harsh environment, BILLI operated practically continuously for nearly a week (from 28 July to 1 August 2016 including an initial instrumental setup phase). During our experiment, the system was placed on a trailer, loaded on a truck, positioned into the courtyard of the INGV (Italian National Institute of Geophysics and Volcanology)observatory "Pizzi Deneri" at 2823 m ASL, on the northeast side of the main crater. This fixed position, about 500 m below the volcano summit, was ≈3 km far from the most important craters [42]. Changing the elevation angle in the range 7–14° while fixing the azimuth angle (230°), BILLI vertically scanned the plume. Atmospheric profiles were recorded every 10 s, whereas each scan, obtained combining 24 profiles, was completed in ~15 min.

Taking into account the local conditions, both the setup (e.g., ON/OFF wavelengths) of the system and the data processing routine remained the same as the previous campaign, with the only exception of a reduction in the system weight (thanks to a rearrangement of the mechanical frame of the system). For these reasons, in this case, laser beam also reached longer ranges and the systematic uncertainty remained stable at 5.5%, whereas, as reported in the literature [39], the statistical uncertainty of lidar profiles increased with range. At 2.5 km, a mean range, it was about 2% [41,42], while it exceeded 5% at 4.2 km [42]. Thanks to the measures already adopted in the previous campaign and reported in Section 2.1, the field setup at Mt. Etna, and the good weather conditions, a slight improvement in the system performances was observed.

Thanks to the BRIDGE DIAL technique, it was possible to retrieve up to 220 scans (lasting 10–20 min) of CO_2 concentration in excess in the plume and, at the same time, the CO_2 flux time-series. The whole dataset covered six days of operation, for a maximum of 12 consecutive hours. Examples of CO_2 profiles, dispersion maps, and flux time-series are reported in Figure 5a–c, in that order [40].

During the campaign, several configurations of plume were recognized, which varied as a function of acquisition time. In fact, both the magnitude and the size of the CO_2 plume were subject to change with the elevation of the laser beam pointing angle and, obviously, they were also influenced by the presence of wind [42].

In general, for elevation angle values comprised within 7° and 9°, it was quite common to detect narrow plume peaks (extending for about 500 m with magnitude values not exceeding 140 ppm) attached or strictly close to the first or the second rockface of Mt. Etna. In fact, at that elevation angle range, the laser beam altitude was lower than the summit crater. Therefore, the profiles' behavior could be justified by the proximity of the rockface behind the plume that, de facto, prevented the complete dispersion of the volcanic cloud into the atmosphere and, at the same time, made the wind contribution negligible.

The situation changed by increasing the elevation angle, as is shown by the profile reported in Figure 5a, which was acquired in the free atmosphere at 15:19 (local civil time) with a 12° elevation angle and a 230° azimuth angle [42]. In Figure 5a, it is possible to note two peaks, relative to CO_2 plume, highlighted by the red boxes. As expected from previous considerations, the first peak, localized between 1250 and 2550 m, was extremely wide (it extends for more than 1 km) and its magnitude exceeded the value of 150 ppm. Instead, the second plume peak, around 250 ppm, was detected beyond 4 km (precisely from 4060 m to 4140 m) from the system location and represents the farthest

plume peak ever detected by our system. The magnifications of both plumes are clearly visible in the lower part of the figure. The measurement uncertainty (obtained by the quadratic sum of both statistical and systematic uncertainties) is equal to 6% and 7.5%, respectively [42]. Instead, the portion of the profile between the two mentioned plume peaks showed several oscillations. These latter were due to the residual presence of instrument noise. For this reason, it was neglected. The behavior of this plume could be justified by the fact that, for such elevation angles and altitudes, the plume was completely dispersed in the free atmosphere and scattered by a moderate presence of the wind [42].

Figure 5b shows an example of CO_2 dispersion vertical map, acquired on 31 July 2016, from 12:47 p.m. to 1:03 p.m. This time slot was selected for the relevance of the results. The tomography represents the in-plume concentration exceedance as a function of elevation angle and range of acquisition. The time evolution of the plume is clearly visible, highlighted by the red, orange, yellow, and green spots with respect to the dark blue color that, instead, represents the CO_2 concentration of the natural background. As already stressed, at lower elevation angles, the plume was circumscribed between the first and second rockface of Mt. Etna encountered by the laser beam. The rockface regions have been highlighted by the semitransparent yellow dotted boxes in the lower side of each scan. Instead, in the free atmosphere, the smoke plume rose and developed in both the vertical and horizontal direction, covering a wide area, after a complete random dispersion. Plume fluctuations in the free atmosphere were also probably due to a combination of the thermal updraft, from the main degassing vents on the volcano summit, and on a smaller scale, to the presence of northwest wind blowing during the measurement session. Furthermore, differences between subsequent maps were also probably due to rapid, local, and random fluctuations of particles and gases emitted by the volcano [42].

Dispersion maps such as the one shown in Figure 5b provide the basis for the computation of the volcanic carbon dioxide flux. In Figure 5c, an example of CO_2 flux series, lasting 6 h (from 12:22 p.m. to 6:08 p.m. local civil time), is reported. As in the Stromboli volcano campaign, CO_2 flux was obtained by multiplying the plume transport velocity with the plume CO_2 molecular density. The first term was obtained with a permanent UV camera network, while the second one was inferred by summing the carbon dioxide excess over the cross section of the volcanic plume [42]. Then, following the procedure reported in Section 2.2.4, it was possible to retrieve the CO_2 flux. The CO_2 flux varied from 13 to 92 kg/s (1235 to more than 8000 tons/day) during the measurement interval, with an average value of 40 ± 13 kg/s (3900 ± 1287 tons/day). The bars in Figure 5c show the CO_2 flux errors (≈30%), and were calculated propagating the errors of plume velocity and CO_2 concentration (procedure detailed in [41,42]). The northeast crater exhibited quiescent degassing during the whole lidar operation. For this reason, the usual variations in degassing were regarded as a consequence of the fluctuations in the magma/gas transport rate occurring in the feeding conduits of Mt. Etna [42].

In order to add confidence to our results, the lidar-based CO_2 flux time-series were compared with independent measurements based on the usual techniques that involve determinations of SO_2 fluxes and CO_2/SO_2 ratios relative to the plume. The averaged values of CO_2 flux retrieved by conventional techniques was found to be equal to about 2750 ktons/day, in good agreement with our measurements. Furthermore, our CO_2 flux time-series (see Figure 5c) were found to be close to the historical time-series retrieved by independent in situ observations: at Mt. Etna, on average, more than 2 ktons/day of carbon dioxide are outputted every day in periods of quiescent passive degassing, while its carbon dioxide emission rates were from 10 to 40 times larger during the effusive event of 2004–2005 [42].

In conclusion, the great novelty, with respect to the previous works [21,37–41], was that our measurements allowed us to locate and track volcanic plumes beyond 4 km of distance from the system location with a lower uncertainty level with respect to the first field tests. In addition, our detected values in excess of CO_2 concentration were consistent with both the conventional measurements (according to volcanologists information) carried out in the same time interval, and with the previous ones acquired during the Stromboli campaign [39–42].

The results reported in this section can be considered to be extremely promising to validate the reliability and accuracy of our system. Furthermore, they represent a further step forward in ground-based volcano monitoring and volcanological research.

4. Conclusions

The main goal of this paper was to show the potential of mobile DIAL-Lidar systems for volcanological research such as the one reported in this work, designed for the remote measurement of both in-plume exceedance of volcanic CO_2 concentration and flux, considered as precursors of volcanic eruptions. Considering the difficulties and, in some circumstances, the hazardousness in retrieving these parameters as well as the limits of conventional in situ instruments, the BILLI system and the related BRIDGE DIAL data analysis technique have been developed. Here, particular emphasis has been placed on the data collection and processing techniques, and the most significant findings of the experimental campaigns carried out over three years at the most hazardous Italian volcanic areas.

Observing the results related to the three experimental campaigns, carried out from October 2014 to July 2016, it is possible to note a gradual refinement of the system performance and an improvement in the accuracy of results. In fact, the implementation of the photo-acoustic cell has made it possible to reduce the systematic uncertainty of CO_2 concentrations to 5.5% and to evaluate a cumulative CO_2 measurement uncertainty (considering both the statistical and systematic uncertainty) between 6% and 7.5%.

The reported approach for the analysis of acquired data allowed us to retrieve, accurately and rapidly, range-resolved CO_2 concentration profiles and maps. Furthermore, and with the aim to improve the already high potential of our system, a further data processing routine was implemented and tested for independent measurements of the plume transport velocity. Nevertheless, this technique, although promising, still requires efforts to be refined. In this way, BILLI will be able to perform simultaneously measurements of CO_2 concentration, CO_2 flux and wind velocity, without additional costs or the support of other conventional devices for the same purpose.

Both CO_2 concentration profiles and maps are fundamental to describe the spatio-temporal dispersion of the volcanic plume into the atmosphere. CO_2 flux time-series retrieved by BILLI (affected by an overall uncertainty of $\approx$25%) were extremely useful to volcanologists for a fast tracking of volcanic activity, particularly if compared with conventional acquisitions.

The detected values in excess of CO_2 concentrations and fluxes were in good agreement with conventional measurements, carried out in the same time interval, but based on completely independent and significantly different approaches. This has proven the sensitivity and reliability of our system for the detection and monitoring of CO_2, not only in limited areas, but also over extended regions and for prolonged periods of time.

In summary, the novelty/advantage of this work is that the proposed standoff DIAL system allows effective measurements (CO_2 excess of a few tens of ppm has been clearly detected) to be taken continuously and remotely (up to more than 4 km from the crater), therefore, from a safer location free from the risks to which operators are exposed during direct sampling. In addition, data have been acquired with much higher temporal (10 s) and spatial (5 m) resolution than conventional instruments (the plume was scanned in few minutes rather than over several hours). Then, a complete time-resolved plume evolution has been detected in several measurement sessions; this can be useful for the assessment of the wind velocity, a crucial parameter not only for the CO_2 flux retrieval, but also for air traffic control applications. These performances allow the operator to characterize the spatio-temporal evolution of the plume, thus providing—24 h and real time—accurate information on an important precursor of eruptions.

To our knowledge, our system performed, for the first time, range-resolved measurements of CO_2 concentration and flux in a volcanic plume and the findings reported laid down the basis for a new and smarter generation of active optical devices, specifically conceived for long-term volcanic gas observation. Even though several improvements have been made (high distances reached, fully

automated operational routines, reduction of system weight, and independent measurements of wind velocity), further developments are still necessary before DIAL-Lidar systems can become operative tools for real-time volcano monitoring. Efforts will have to be made, in particular, to improve portability (the current system weight is about 1100 kg), to reduce power requirements (currently, 6.5 KW) and to integrate existing system control and data processing routines to create a unique, user-friendly, and fully automated software framework for the end-users.

In the near future, it will be desirable to deploy both ground-based (using a newly designed laser-based system such as the one described in this paper together with conventional sensors) and airborne (or space borne) platforms, forming a robust, integrated network for eruptions forecasting for prolonged periods. This will allow us to provide useful information to volcanologists, concerning the time evolution of volcanic gases in hazardous regions while working remotely and safely.

Conflicts of Interest: The authors declare no conflict of interest.

References

1. Paik, S.; Min, S.K. Assessing the Impact of Volcanic Eruptions on Climate Extremes Using CMIP5 Models. *J. Clim.* **2018**, *31*, 5333–5349. [CrossRef]
2. Sparks, R.S.J.; Biggs, J.; Neuberg, J.W. Monitoring Volcanoes. *Science* **2012**, *335*, 1310–1311. [CrossRef] [PubMed]
3. Chouet, B.; Matoza, R. A multi-decadal view of seismic methods for detecting precursors of magma movement and eruption. *J. Volcanol. Geotherm. Res.* **2013**, *252*, 108–175. [CrossRef]
4. Dzurisin, D. A comprehensive approach to monitoring volcano deformation as a window on the eruption cycle. *Rev. Geophys.* **2003**, *41*, 1001–1030. [CrossRef]
5. Biggs, J.; Ebmeier, S.K.; Aspinall, W.P.; Lu, Z.; Pritchard, M.E.; Sparks, R.S.J.; Mather, T.A. Global link between deformation and volcanic eruption quantified by satellite imagery. *Nat. Commun.* **2014**, *5*, 3471. [CrossRef]
6. Iverson, R.M.; Dzurisin, D.; Gardner, C.A.; Gerlach, T.M.; Lahusen, R.G.; Lisowski, M.; Major, J.; Malone, S.D.; Messerich, J.A.; Moran, S.C.; et al. Dynamics of seismogenic volcanic extrusion at Mount St Helens in 2004–05. *Nature* **2006**, *444*, 439–443. [CrossRef]
7. Aiuppa, A. Volcanic gas monitoring. In *Volcanism and Global Environmental Change*; Schmidt, A., Fristad, K.E., Elkins-Tanton, L.T., Eds.; Cambridge University Press: Cambridge, UK, 2015.
8. Oppenheimer, C.; Fischer, T.; Scaillet, B. Volcanic Degassing: Process and Impact. In *Treatise on Geochemistry*, 2nd ed.; Holland, H.D., Turekian, K.K., Eds.; Elsevier: Oxford, UK, 2014; Volume 4, pp. 111–179. [CrossRef]
9. Edmonds, M. New geochemical insights into volcanic degassing. *Philos. Trans. R. Soc. A* **2008**, *366*, 1885. [CrossRef]
10. Aiuppa, A.; Burton, M.; Caltabiano, T.; Giudice, G.; Guerrieri, S.; Liuzzo, M.; Murè, F.; Salerno, G. Unusually large magmatic CO_2 gas emissions prior to a basaltic paroxysm. *Geophys. Res. Lett.* **2010**, *37*. [CrossRef]
11. Burton, M.R.; Sawyer, G.M.; Granieri, D. Deep Carbon Emissions from Volcanoes. *Rev. Miner. Geochem.* **2013**, *75*, 323–354. [CrossRef]

12.   Werner, C.; Fischer, T.P.; Aiuppa, A.; Edmonds, M.; Cardellini, C.; Carn, S.; Chiodini, G.; Cottrell, E.; Burton, M.; Shinohara, H.; et al. Carbon dioxide emissions from subaerial volcanic regions: Two decades in review. In *Deep Carbon Past to Present*; Orcutt, B.N., Daniel, I., Dasgupta, R., Eds.; Cambridge University Press: Cambridge, UK, 2019; Volume 8, pp. 188–236.

13.   Fischer, T.P.; Arellano, S.; Carn, S.; Aiuppa, A.; Galle, B.; Allard, P.; Lopez, T.; Shinohara, H.; Kelly, P.; Werner, C.; et al. The emissions of CO_2 and other volatiles from the world's subaerial volcanoes. *Sci. Rep.* **2019**, *9*, 18716. [CrossRef]

14.   Queißer, M.; Burton, M.; Kazahaya, R. Insights into geological processes with CO_2 remote sensing—A review of technology and applications. *Earth Sci. Rev.* **2019**, *188*, 389–426. [CrossRef]

15.   Platt, U.; Bobrowski, N.; Butz, A. Ground-Based Remote Sensing and Imaging of Volcanic Gases and Quantitative Determination of Multi-Species Emission Fluxes. *Geosciences* **2018**, *8*, 44. [CrossRef]

16.   Oppenheimer, C. Ultraviolet sensing of volcanic sulfur emissions. *Elements* **2010**, *6*, 87–92. [CrossRef]

17.   Theys, N.; Hedelt, P.; De Smedt, I.; Lerot, C.; Yu, H.; Vlietinck, J.; Pedergnana, M.; Arellano, S.; Galle, B.; Fernandez, D.; et al. Global monitoring of volcanic SO_2 degassing with unprecedented resolution from TROPOMI onboard Sentinel-5 Precursor. *Sci. Rep.* **2019**, *9*, 2643. [CrossRef] [PubMed]

18.   Carn, S.; Fioletov, V.E.; McLinden, C.A.; Li, C.; Krotkov, N.A. A decade of global volcanic SO_2 emissions measured from space. *Sci. Rep.* **2017**, *7*, 44095. [CrossRef] [PubMed]

19.   Allard, P.; Burton, M.R.; Mure, F. Spectroscopic evidence for a lava fountain driven by previously accumulated magmatic gas. *Nature* **2005**, *433*, 407–410. [CrossRef]

20.   Fischer, T.P.; Chiodini, G. Volcanic, Magmatic and Hydrothermal Gas Discharges. In *Encyclopedia of Volcanoes*, 2nd ed.; Sigurdsson, H., Houghton, B., McNutt, S., Rymer, H., Stix, J., Eds.; Elsevier: Amsterdam, The Netherlands, 2015; pp. 779–797. [CrossRef]

21.   Aiuppa, A.; Fiorani, L.; Santoro, S.; Parracino, S.; Nuvoli, M.; Chiodini, G.; Minopoli, C.; Tamburello, G. New ground-based lidar enables volcanic CO_2 flux measurements. *Sci. Rep.* **2015**, *5*, 13614. [CrossRef]

22.   Conde, V.; Robidoux, P.; Avard, G.; Galle, B.; Aiuppa, A.; Muñoz, A.; Giudice, G. Measurements of SO_2 and CO_2 by combining DOAS, Multi-GAS and FTIR: Study cases from Turrialba and Telica volcanoes. *Int. J. Earth Sci.* **2014**, *103*, 2335–2347. [CrossRef]

23.   Saccorotti, G.; Iguchi, M.; Aiuppa, A. In situ Volcano Monitoring: Present and Future in Volcanic Hazards, Risks and Disasters. In *Volcanic Hazards, Risks, and Disasters*; Shroder, J.F., Papale, P., Eds.; Elsevier: Amsterdam, The Netherlands, 2014; Volume 202, p. 169. [CrossRef]

24.   Symonds, R.B.; Rose, W.I.; Bluth, G.J.S.; Gerlach, T.M. Volcanic-gas studies: Methods, results and applications. *Rev. Mineral.* **1994**, *30*, 1–66.

25.   Aiuppa, A.; Fischer, T.P.; Plank, T.; Bani, P. CO_2 flux emissions from the Earth's most actively degassing volcanoes, 2005–2015. *Sci. Rep.* **2019**, *9*, 5442. [CrossRef]

26.   Aiuppa, A.; Giudice, G.; Gurrieri, S.; Liuzzo, M.; Burton, M.; Caltabiano, T.; Mcgonigle, A.J.S.; Salerno, G.; Shinohara, H.; Valenza, M. Total volatile flux from Mount Etna. *Geophys. Res. Lett.* **2008**, *35*, L24302. [CrossRef]

27.   Casadevall, T.J.; Rose, W.I.; Fuller, W.H.; Hunt, W.H.; Hart, M.A.; Moyers, J.L.; Woods, D.C.; Chuan, R.L.; Friend, J.P. Sulfur Dioxide and Particles in Quiescent Volcanic Plumes from Poàs, Arenal, and Colima Volcanos, Costa Rica and Mexico. *J. Geophys. Res.* **1984**, *89*, 9633–9641. [CrossRef]

28.   Edner, H.; Ragnarson, P.; Wallinder, E.; Ferrara, R.; Cioni, R.; Taddeucci, G.; Svanberg, S.; Raco, B. Total fluxes of sulfur dioxide from the Italian Volcanoes Etna, Stromboli and Vulcano measured by differential absorption lidar and passive differential optical absorption spectroscopy. *J. Geophys. Res.* **1994**, *99*, 18827–18838. [CrossRef]

29.   Porter, J.N.; Horton, K.A.; Mouginis-Mark, P.J.; Lienert, B.; Sharma, S.K.; Lau, E.; Sutton, A.J.; Elias, T.; Oppenheimer, C. Sun photometer and lidar measurements of the plume from the Hawaii Kilauea Volcano Pu'u O'o vent: Aerosol flux and SO_2 lifetime. *Geophys. Res. Lett.* **2002**, *29*, 30–34. [CrossRef]

30.   Hobbs, P.V.; Radke, L.F.; Lyons, J.H.; Ferek, R.J.; Coffman, D.J.; Casadevall, T.J. Airborne measurements of particle and gas emissions from the 1990 volcanic eruptions of Mount Redoubt. *J. Geophys. Res.* **1991**, *96*, 18735–18752. [CrossRef]

31.   Fiorani, L.; Colao, F.; Palucci, A. Measurement of Mount Etna plume by CO_2-laser-based lidar. *Opt. Lett.* **2009**, *34*, 800–802. [CrossRef]

32. Jäger, H. The Pinatubo eruption cloud observed by lidar at Garmisch-Partenkirchen. *Geophys. Res. Lett.* **1992**, *19*, 191–194. [CrossRef]

33. Weibring, P.; Edner, H.; Svanberg, S.; Cecchi, G.; Pantani, L.; Ferrara, R.; Caltabiano, T. Monitoring of volcanic sulphur dioxide emissions using differential absorption lidar (DIAL), differential optical absorption spectroscopy (DOAS), and correlation spectroscopy (COSPEC). *Appl. Phys. B* **1998**, *67*, 419–426. [CrossRef]

34. Fiorani, L.; Colao, F.; Palucci, A.; Poreh, D.; Aiuppa, A.; Giudice, G. First-time lidar measurement of water vapor flux in a volcanic plume. *Opt. Commun.* **2011**, *284*, 1295–1298. [CrossRef]

35. Winker, D.M.; Liu, Z.; Omar, A.; Tackett, J.; Fairlie, D. CALIOP observations of the transport of ash from the Eyjafjallajökull volcano in April 2010. *J. Geophys. Res.* **2012**, *117*, D00U15. [CrossRef]

36. Fiorani, L.; Aiuppa, A.; Angelini, F.; Borelli, R.; Del Franco, M.; Murra, D.; Pistilli, M.; Puiu, A.; Santoro, S. Lidar sounding of volcanic plumes. In Proceedings of the SPIE 8894, Lidar Technologies, Techniques, and Measurements for Atmospheric Remote Sensing IX, Dresden, Germany, 22 October 2013; p. 889407. [CrossRef]

37. Fiorani, L.; Santoro, S.; Parracino, S.; Nuvoli, M.; Minopoli, C.; Aiuppa, A. Volcanic CO_2 detection with a DFM/OPA-based lidar. *Opt. Lett.* **2015**, *40*, 1034–1036. [CrossRef] [PubMed]

38. Fiorani, L.; Santoro, S.; Parracino, S.; Maio, G.; Del Franco, M.; Aiuppa, A. Lidar detection of carbon dioxide in volcanic plumes. In Proceedings of the SPIE 9535, Third International Conference on Remote Sensing and Geoinformation of the Environment (RSCy2015), 95350N, Paphos, Cyprus, 19 June 2015. [CrossRef]

39. Fiorani, L.; Santoro, S.; Parracino, S.; Maio, G.; Nuvoli, M.; Aiuppa, A. Early detection of volcanic hazard by lidar measurement of carbon dioxide. *Nat. Hazards* **2016**, *83*, S21–S29. [CrossRef]

40. Parracino, S.; Santoro, S.; Maio, G.; Nuvoli, M.; Aiuppa, A.; Fiorani, L. Fast tracking of wind velocity with a differential absorption LiDAR system: First results of an experimental campaign at Stromboli volcano. *Opt. Eng.* **2017**, *56*. [CrossRef]

41. Aiuppa, A.; Fiorani, L.; Santoro, S.; Parracino, S.; D'Aleo, R.; Liuzzo, M.; Maio, G.; Nuvoli, M. New Advances in Dial-Lidar-based remote sensing of the volcanic CO_2 flux. *Front. Earth Sci.* **2017**, *5*, 15. [CrossRef]

42. Santoro, S.; Parracino, S.; Fiorani, L.; D'Aleo, R.; Di Ferdinando, E.; Giudice, G.; Maio, G.; Nuvoli, M.; Aiuppa, A. Volcanic Plume CO_2 Flux Measurements at Mount Etna by Mobile Differential Absorption Lidar. *Geosciences* **2017**, *7*, 9. [CrossRef]

43. Fiorani, L. Lidar application to litosphere, hydrosphere and atmosphere. In *Progress in Laser and Electro-Optics Research*; Koslovskiy, V.V., Ed.; Nova: New York, NY, USA, 2010; pp. 21–75.

44. Kovalev, V.; Eichenger, W.E. *Elastic Lidar, Theory, Practice and Analysis Methods*; Wiley & Sons, Inc.: Hoboken, NJ, USA, 2004.

45. Gordon, I.E.; Rothman, L.S.; Hill, C.; Kochanov, R.; Tan, Y.; Bernath, P.; Birk, M.; Boudon, V.; Campargue, A.; Chance, K.; et al. The HITRAN 2016 molecular spectroscopic database. *J. Quant. Spectrosc. Radiat. Transf.* **2017**, *203*, 3–69. [CrossRef]

46. Schafer, R.W. What Is a Savitzky-Golay Filter? *IEEE Signal Process Mag.* **2011**, *28*, 111–117. [CrossRef]

47. Eloranta, E.W.; King, J.M.; Weinman, J.A. The determination of wind velocitys in the boundary layer by monostatic LiDAR. *J. Appl. Meteor.* **1975**, *14*, 1485–1489. [CrossRef]

48. Papoulis, A.; Pillai, U. *Probability, Random Variables and Stochastic Processes*, 4th ed.; McGraw-Hill: New York, NY, USA, 2002.